

Smoke and Mirrors: demonstrating interferometry on synthetic converted wave data

David C. Henley

ABSTRACT

Over the last several years, we have developed and demonstrated techniques for removing the near-surface effects (statics) from seismic traces, using interferometric methods, and have shown how to generalize constraints like surface-consistency and stationarity. We have shown significant results using field data from the Canadian arctic. More recently, we have adapted these methods to converted wave data, where the receiver corrections are difficult to determine using conventional methods. This work illustrates the testing of interferometric methods on several related synthetic models, each designed to isolate and study a particular issue raised by converted wave interferometry. We introduce various procedures for improving our results, and show them in practice on the model data. Our insight for dealing with real data has been significantly increased by the study.

INTRODUCTION

The use of interferometric techniques in seismic data processing has increased dramatically over the last few years, and new applications appear frequently in the technical literature (Wapenaar et al 2006). A few years ago, we developed a method called “statics deconvolution” for removing the near-surface time delay and phase effects from seismic traces (Henley 2004, 2005, 2006). Subsequent comparison of our method with some of the emerging interferometry techniques revealed many similarities; hence, we include statics deconvolution under the broad category of interferometric methods.

We searched for new ideas and inspiration in the interferometry literature, and improved our own technique as a consequence. During our development, we had access to two field data sets from the Canadian arctic, each of them posing unique problems for near-surface corrections. On one of these, the Hansen Harbour survey, we compared our statics deconvolution method with a modified version of the ‘virtual source’ method of Bakulin and Calvert (2006) with favourable results (Henley and Daley 2007); and tested the rudiments of our ‘raypath interferometry’ method (Henley 2006, 2008). In this method we abandon the constraint of ‘surface-consistency’ for a more general one of ‘raypath-consistency’. The first full-blown test of raypath interferometry was its application to a problem data set from the MacKenzie Delta, loaned to us by Shell Canada (Henley 2006, 2008). The success of the method on these data led us to attempt next to apply it to the significant problem of determining receiver corrections for converted wave (PS) data (Henley and Daley 2008). In spite of the overall good quality of the field data we used in tests (Spring Coulee survey) the method was only partially successful. It proved to be more difficult to construct ‘pilot traces’ from the raw data than anticipated, one of the key tasks in the procedure.

An innovative presentation at the 2009 CSPG/CSEG joint convention (DeMeersman and Roizman 2009), helped germinate the next idea for our development efforts. In their

technique, these authors cross-correlated vertical component direct arrival events with the direct arrival events (converted at the base of weathering) from the corresponding radial component to find the relative time shifts between them. The resulting ‘receiver functions’ were then analyzed for the difference between the PP receiver static and PS receiver static at each surface location. Instead of cross-correlating the direct arrivals of corresponding PP and PS direct arrivals, however, we decided to cross-correlate corresponding reflected and converted events, in a technique which we call ‘hybrid interferometry’; and furthermore, to use the cross-correlations not just to find delay times, but to derive inverse filters for removing the shifts/phase differences by deconvolution. In other words, we wished to use the vertical component reflected data as ‘pilot traces’ for the radial component ‘converted wave’ data.

We began our testing with the same data set used by DeMeersman and Roizman: Spring Coulee. There is no particular evidence that surface-consistency is violated in this area, so our more general raypath-consistent approach (Henley 2006, 2008) may not be strictly required. We chose to apply it nevertheless, because the process of transforming the data to common-angle gathers often enhances the S/N ratio over some range of common-angle gathers, allowing more robust solutions from the gathers representing those angles. By over-sampling in the angle (apparent velocity) domain when performing the radial trace transform, we get the benefit of redundancy, as well, in the common-angle domain, which can make solutions more robust in the presence of noise.

A companion report chapter (Henley 2009) shows the results of our testing of ‘hybrid interferometry’, based on ‘statics deconvolution’ and ‘raypath interferometry’ on the Spring Coulee 2D-3C data; but several questions arose during our testing that could not be answered from our tests on field data alone. Thus it seemed appropriate to apply the statics deconvolution method, as well as the raypath consistency concept, to synthetic seismic models of varying complexity, in order to evaluate these questions:

- Can we reliably correct PS events for the receiver side near-surface effects by using interferometric methods on raw trace gathers?
- When there is more than one strong PP reflected event and/or more than one corresponding PS event, what effect do the secondary correlation peaks have on the inverse filters and the correction of the PS events?
- What techniques can we use to diminish these effects?
- How does random noise degrade the quality of the result?
- How does the raypath interferometry approach compare with simple trace gather interferometry?

In order to answer these questions, we built a series of increasingly complex models as follows:

- Model 1 consists of a PP reflected event gather (vertical component) containing a single flat event, and a corresponding PS event gather (radial

component). On the PS gather, the event on each trace was shifted by a random amount, simulating receiver statics. Neither PP nor PS gathers contained added noise.

- Model 2 consists of the same PP reflected event gather as model 1, but with an additional reflected event, unrelated to the PS event on the second gather. The simulated radial component PS gather was the same as model 1. No noise was added.
- Model 3 embodied two events on each gather. Both events on the PS gather had the same statics, emulating surface-consistency. Only one event on each gather corresponded to an event on the other. No noise was added.
- Model 4 consisted of two gathers; but each contained five events, only one of which corresponded to a related event on the other gather. Once again, no noise was added to either gather.
- Model 5 had the same reflected/converted events as model 4, but a modest level of uncorrelated bandlimited random noise was added to both gathers.
- Model 6 contained the same events as model 5, except that two complete sets of shot gathers (vertical component and radial component) were created, constituting an entire seismic line. An additional complication was the muting of the simulated converted wave events over a range of near offsets to approximately model the diminished PS conversion around normal incidence. A background level of uncorrelated bandlimited random noise was added to all the gathers.

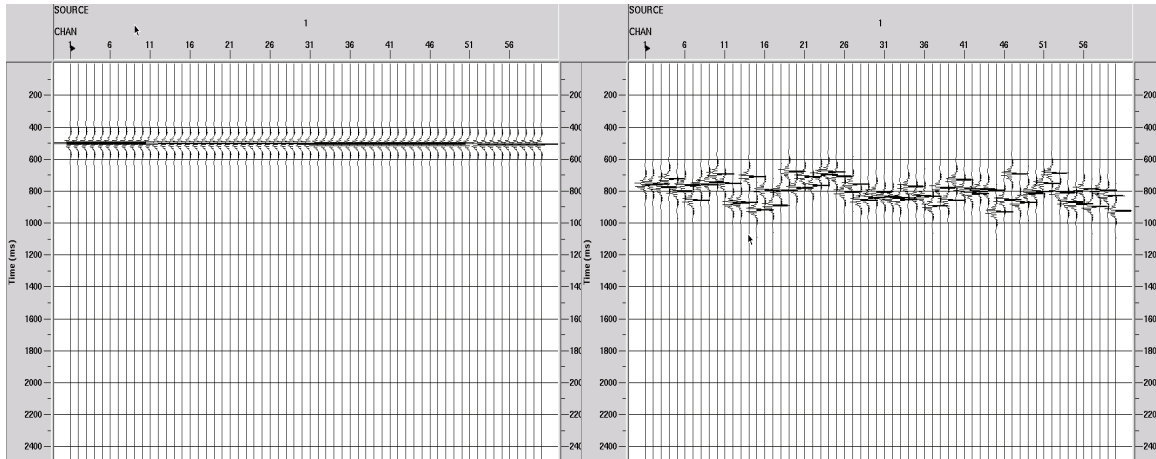
For all tests, it is assumed that PP-wave reflection events have been corrected for near-surface effects, either with standard statics methods or a previous application of statics deconvolution to the vertical component data, prior to using them as pilot traces for the corresponding PS events. Hence the PP-wave model traces have no residual statics, and we further assume no geological structure. When we generated the gathers for each model, we did not attempt to mute early portions of the traces proportionally to their distance from the shot point to emulate the appearance of real gathers, since there are no actual events in this part of the gather on any of the models, including direct arrivals. Likewise, we simulated gathers which are perfectly NMO-corrected (with no stretch). A final simplifying assumption used in all the models was that all events were simple bandlimited spikes—we used no complex interfaces, and we made no attempt to model actual reflectivity vs. ‘convertivity’ on corresponding interfaces. The issue of reflectivity and ‘convertivity’ functions from the same lithological sequence, and how they are related is deferred for future study. The present study is primarily concerned with event timing and relative amplitude, not wavelet shape. The only concession to reality was the use of a narrower frequency band to represent PS events than that used for simulated PP events. None of these models is geological in any real sense.

In the following section, we show results for each of these models and discuss the implications for real data.

MODEL RESULTS

Model 1

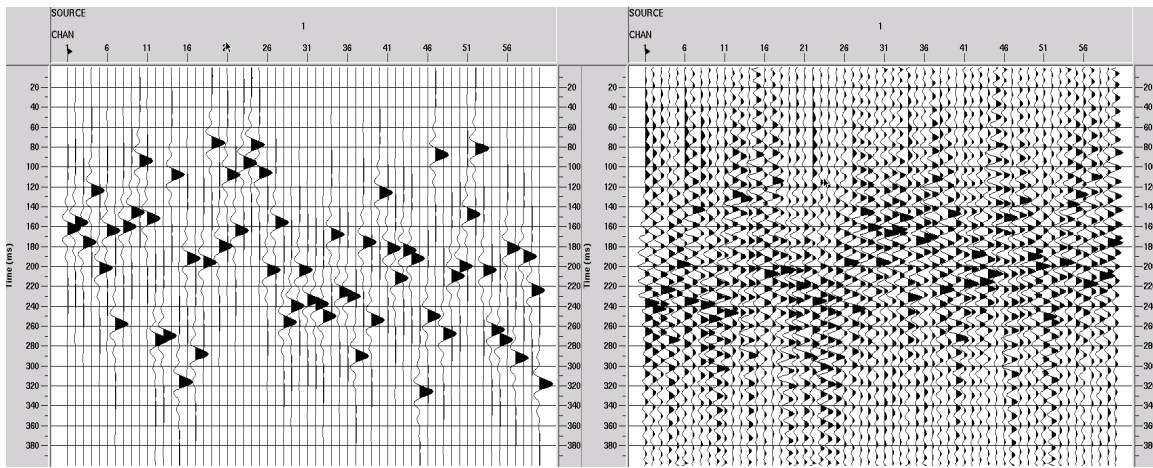
The purpose of Model 1 was to visually validate the basic process of statics deconvolution. Hence, we cross-correlated one simulated PP gather against a simulated PS gather, whose single event is narrower in band, and is perturbed by relatively large random statics (some statics are much larger than the apparent ‘wavelength’ of the converted wave event). Figure 1 shows both model gathers. As can be seen, there is no additive noise. The cross-correlations between events on corresponding P and PS traces are shown in Figure 2, as are the inverse filters derived from the cross-correlations.



Synthetic PP reflected event shot gather

Synthetic PS converted wave shot gather

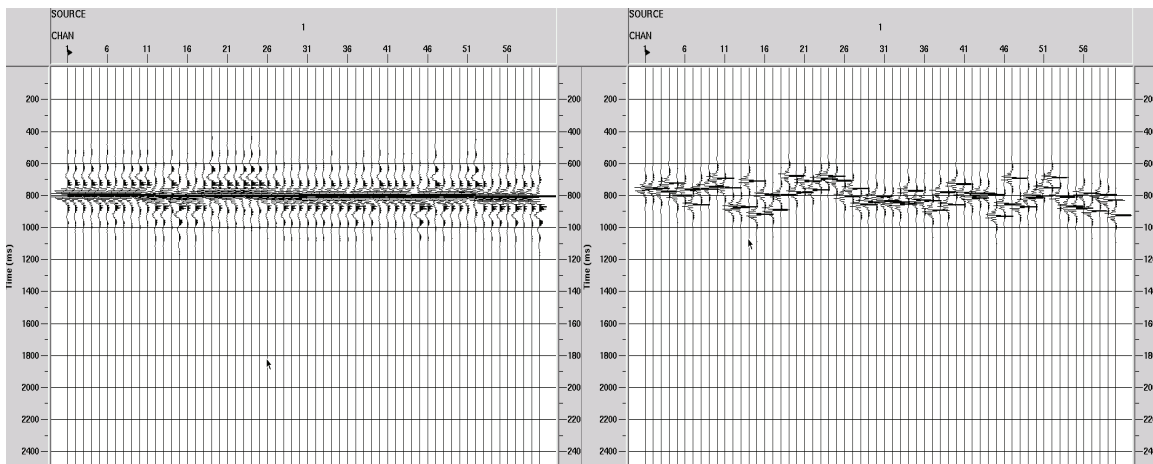
FIG. 1. Model 1—synthetic PP reflected event gather and its corresponding PS converted wave gather with random statics. The receiver for each P trace and its corresponding PS trace is the same.



Cross-correlations, and their corresponding inverse filters, for the PP traces and their corresponding PS traces in Figure 1

FIG. 2. Model 1—cross-correlations between PP and PS traces from Figure 1 (left) and the inverse filters derived from them (right). Note the large trace-to-trace shifts in the correlation peaks, and the long inverse filters required to account for these ‘unconditioned’ correlation functions.

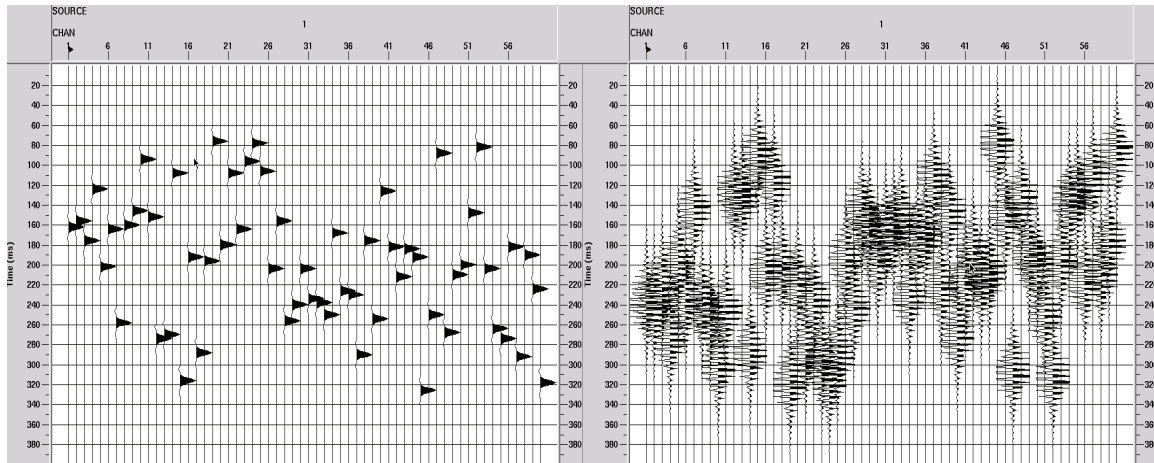
Note that the cross-correlation length is 400 ms (distinct from the window length, which determines the length of the input traces) in order to capture all the statics manifested on the PS traces, some of which are quite large. Note, as well, that the PS event has been uniformly shifted up by 300 ms prior to cross-correlation in order to match its corresponding PP event in time, a necessary step when processing real data, as well. The inverse filters in Figure 2, when applied to their respective PS traces, result in the corrected event in Figure 3 (compared to the original gather with statics).



PS event after application of inverse filters, compared to original gather with statics

FIG. 3. Model 1—PS trace gather corrected by application of the inverse filters in Figure 2 (left), compared with the original PS gather.

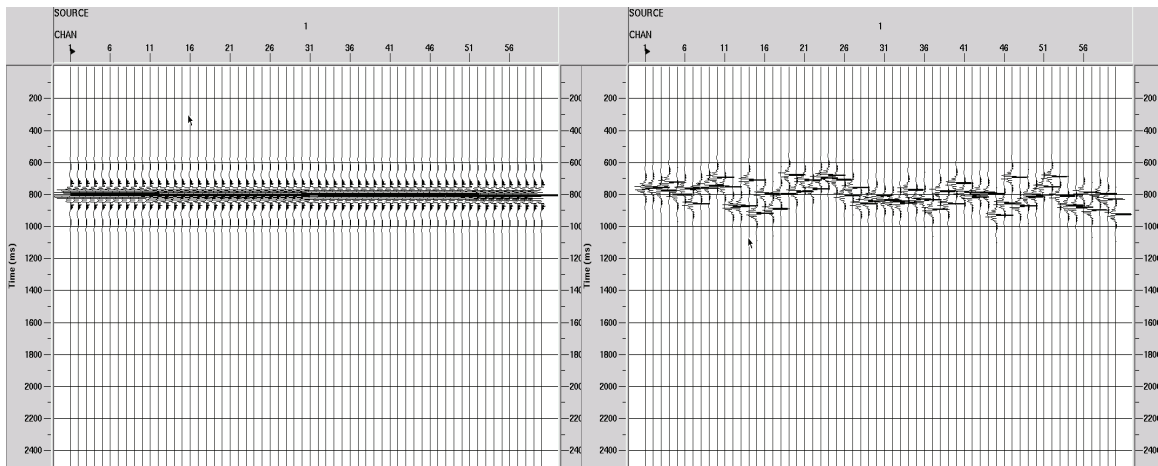
Two effects are evident: the PS traces have been reasonably well corrected for statics; but the PS events have lost bandwidth in the process. We know that a cross-correlation is, by its nature, narrower in band than either of its contributing time series; so we can partially compensate for that by ‘conditioning’ the correlation before deriving its inverse filter. We choose a non-linear conditioning step in which we raise the samples of the cross-correlation to an odd power, and then weight the whole correlation function with a Hanning window. This has the effect of whitening the function without introducing additional peaks, and of de-emphasizing outlying peaks. When we apply this conditioning using an exponent of 5, the cross-correlation functions in Figure 2 become those in Figure 4, with their corresponding inverse filters shown, as well.



Cross-correlations, and their corresponding inverse filters, for the PP traces and their corresponding PS traces in Figure 1. In this case, cross-correlations have been ‘conditioned’ by exponentiating samples to 5 and applying Hanning weights to window.

FIG. 4. Model 1—cross-correlations from Figure 2 after ‘conditioning’ by raising samples to exponent of 5 and applying Hanning weighting to functions (left), and corresponding inverse filters (right). These inverse filters are much broader in band and hence more localized than those in Figure 2.

Note that these filters are much more localized around the net static shift than those in Figure 2. Figure 5 compares the result of deconvolving the original PS gather with these new inverse filters, compared with the original gather. Immediately, we see that the statics have been completely removed, and that more of the bandwidth of the PS event has been preserved, compared to Figure 3.

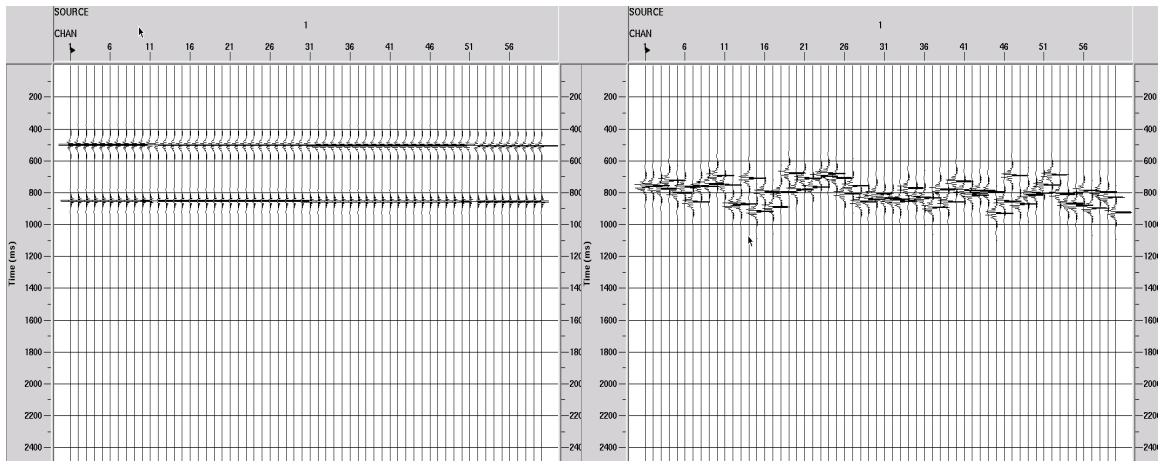


PS event after application of inverse filters, compared to original gather with statics.
 'Conditioned' cross-correlations used for inverse filters.

FIG. 5. Model 1—corrected PS gather (left) vs. original gather (right). This result, obtained using the inverse filters in Figure 4, is much broader band and more uniform in phase than the result in Figure 3.

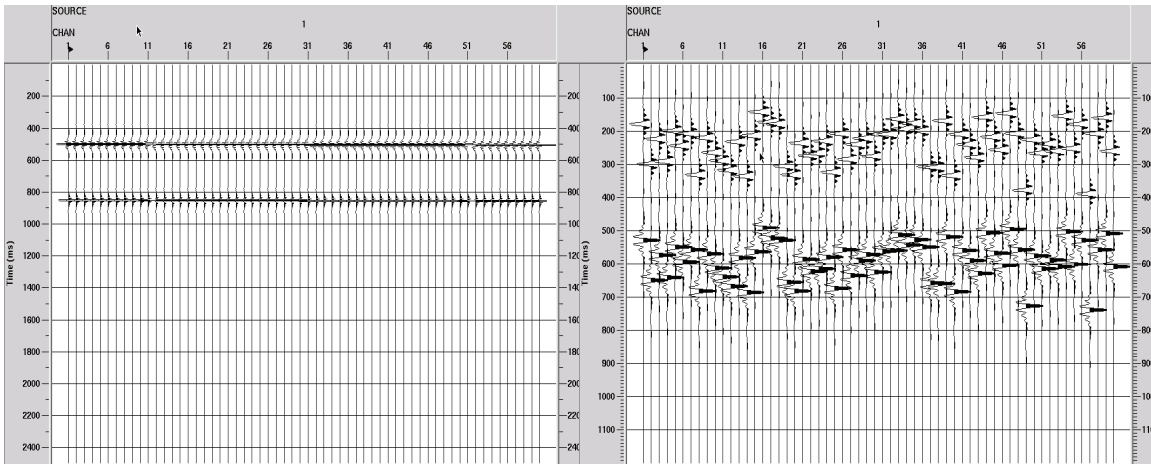
Model 2

Figure 6 shows the simulated PP and PS gathers comprising Model 2. Note that the only difference between this model and the previous one is the addition of a second reflection event to the PP gather, which will lead to secondary peaks in the cross-correlations between PP and PS events. Figure 7 shows the PP gather followed by the correlations, this time with both window length and correlation length of 1200 ms, to deliberately ensure the inclusion of the secondary peaks within the inverse filter derivation window.



Model 2—Two simulated PP reflections vs one simulated PS event with statics

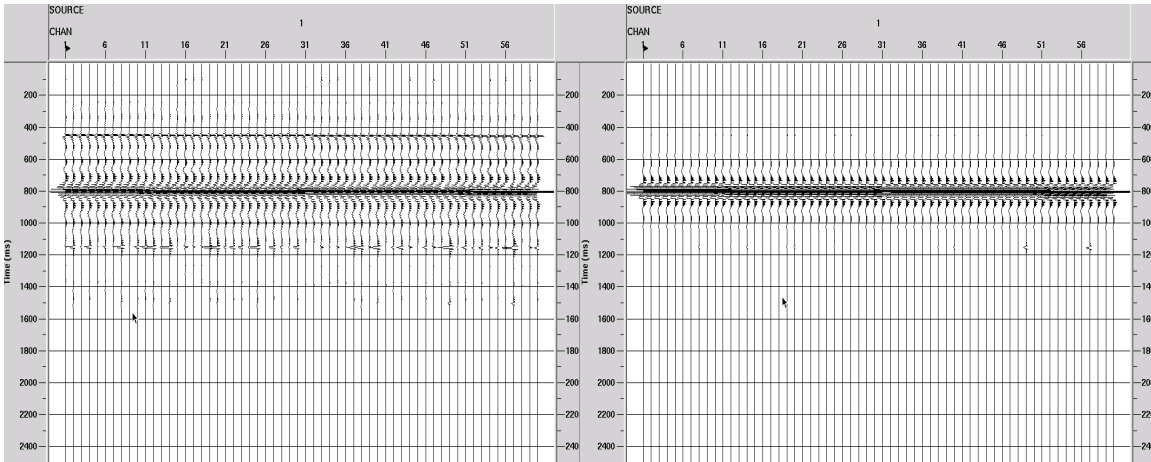
FIG. 6. Model 2—simulated PP reflected event gather with two events (left) vs. simulated PS gather (right), with random statics. The single PS event corresponds to the PP event at 500 ms.



Model 2 reflections and the resulting cross-correlations with the simulated PS event

FIG. 7. Model 2—simulated PP gather (left) vs. the 1200 ms cross-correlation functions between corresponding traces on the PP gather and the single-event PS gather.

Figure 8 shows the result of deriving inverse filters on the unmodified correlation functions and applying them to the raw PS gather, as well as the result of conditioning the correlations before deriving the inverses. This figure makes it obvious that conditioning practically eliminates the influence of a secondary correlation peak on the derivation of the inverse filter and also preserves more of the original PS event bandwidth. This is because the primary correlation is stronger than the secondary one, and is always nearer the centre of the window. If either of these conditions is violated, the effect of conditioning would likely fail.

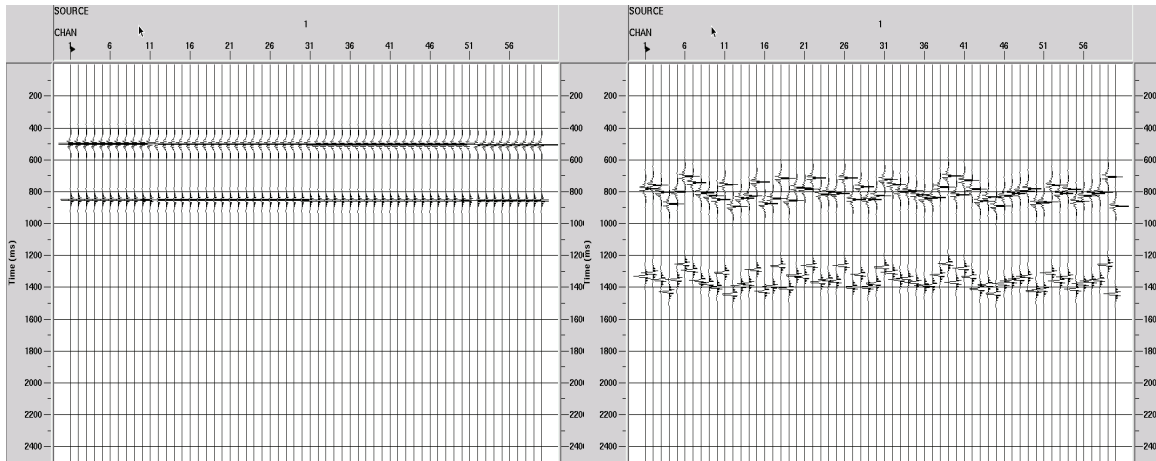


Model 2—deconvolved with inverses from raw correlations vs 'conditioned' correlations

FIG. 8. Model 2—corrected PS gather using inverse filters from raw cross-correlations (left) vs. 'conditioned' cross-correlations (right). Note the attenuation of spurious events when using the conditioned cross-correlations.

Model 3

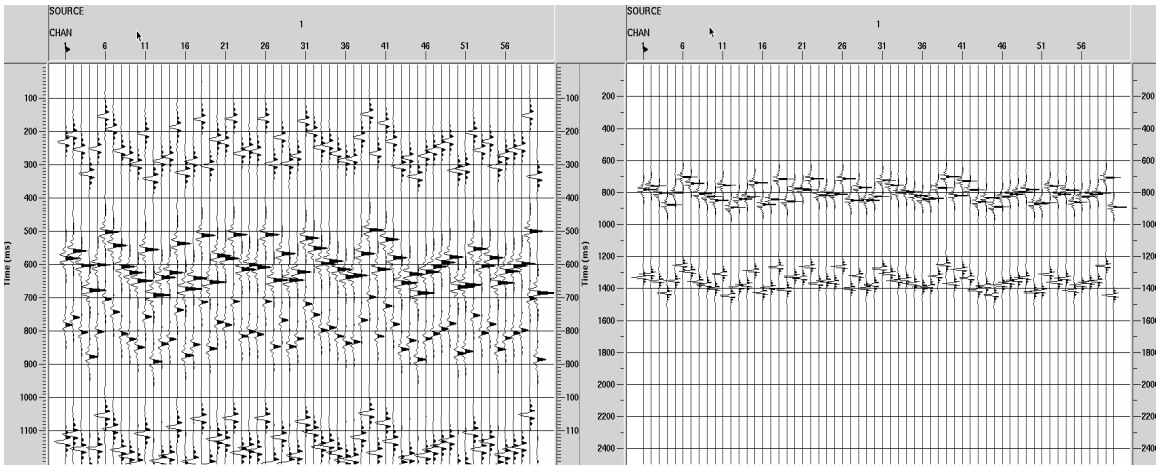
The addition of a second event to the PS gather, as shown in Figure 9, further complicates the problem by introducing more secondary peaks into the cross-correlations between corresponding PP and PS traces. Recall that the PS traces are shifted by 300 ms before cross-correlation, so that the event at 800 ms matches the 500 ms reflection event on the PP gather. We assume that the second PP reflected event does not necessarily correspond to the second PS event, and that even with the 300 ms shift, these events do not match in time (due to presumed lower velocity of the converted wave event).



Model 3—two PP events and two simulated PS events: only one correlated to PP event

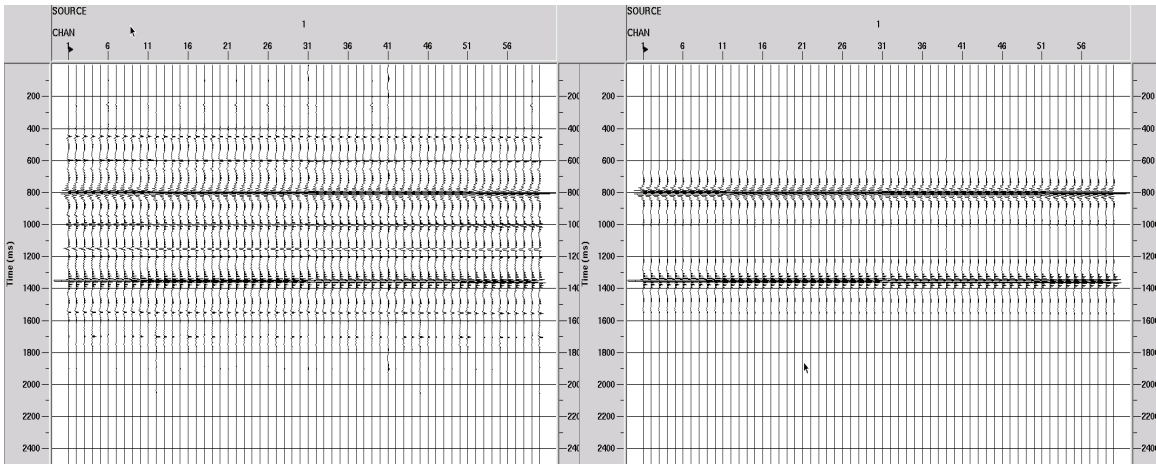
FIG. 9. Model 3—simulated PP reflection gather with two events (left) vs. simulated PS gather, also with two events (right). Only the 500 ms event on the PP gather and the approx. 800 ms event on the PS gather are the same event. Random statics on PS gather affect both events equally, and are thus surface-consistent

Note that the static on each PS trace is the same for both events, implying surface-consistency. The 1200 ms long cross-correlations for these gathers are shown in Figure 10, beside the PS gather. Note that not all of the secondary correlation details are completely captured even with this long correlation (window length is also 1200 ms), but that the majority of the peaks are included. The result of applying inverse filters for the raw correlations, and the conditioned correlations, respectively, are shown in Figure 11. Once again, it is evident that conditioning the correlations before deriving their inverses greatly suppresses spurious events on the deconvolved PS gather, and preserves bandwidth, as well. Nevertheless, this is a simple model with only two events per gather and no added noise.



Model 3 cross-correlations and the simulated raw PS gather

FIG. 10. Model 3—1200 ms long cross-correlations (left) vs. simulated PS gather (right). Note that the 1200 ms correlation length is no longer large enough to capture all the secondary correlation peaks and side-lobes of the cross-correlated trace pairs from Figure 9.

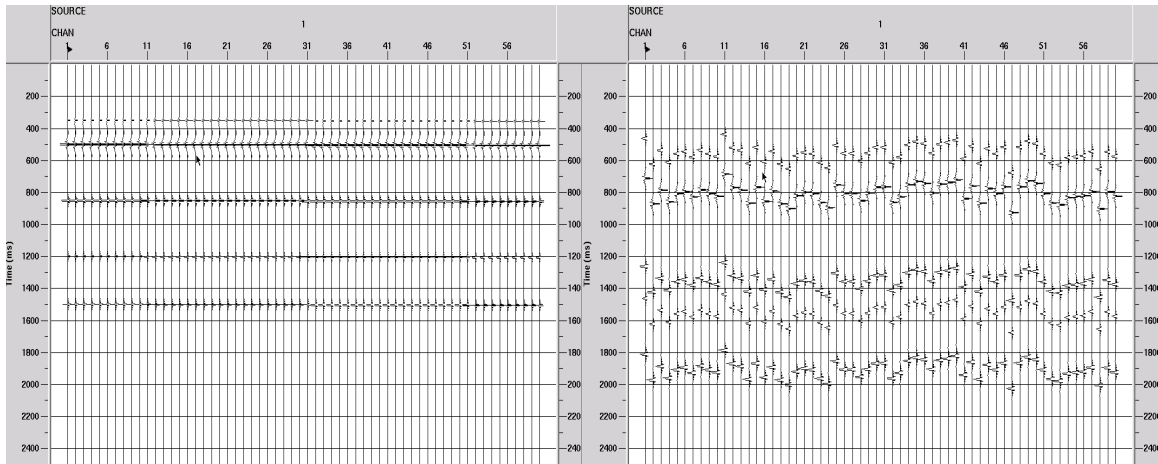


Model 3 simulated PS gather deconvolved using unconditioned cross-correlations (left) vs 'conditioned' correlations (right)

FIG. 11. Model 3—simulated PS gather as corrected by inverse filters derived from unconditioned correlations (left), and 'conditioned' correlations (right). As in Model 2, the conditioning of the correlation functions leads to inverse filters whose application suppresses spurious events on the PS gather, while correcting the embedded statics.

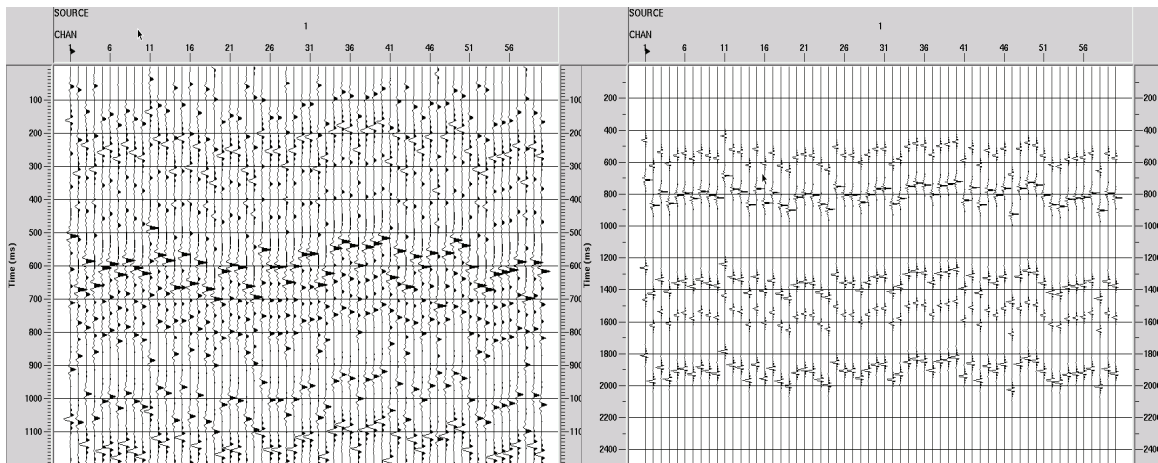
Model 4

Next, we increase the complexity of the model still further by including five events each on both the PP and PS gathers, still with only the PP event at 500 ms matched to a PS event at 800 ms. This model is shown in Figure 12. As in the previous model, all events on a single PS trace share a common static, preserving surface-consistency. The PS gather and the cross-correlations with the PP gather are shown in Figure 13.



Model 4—five simulated PP events vs five simulated PS events with statics. Only the PP event at 500 ms and the PS event at 800 ms are matched.

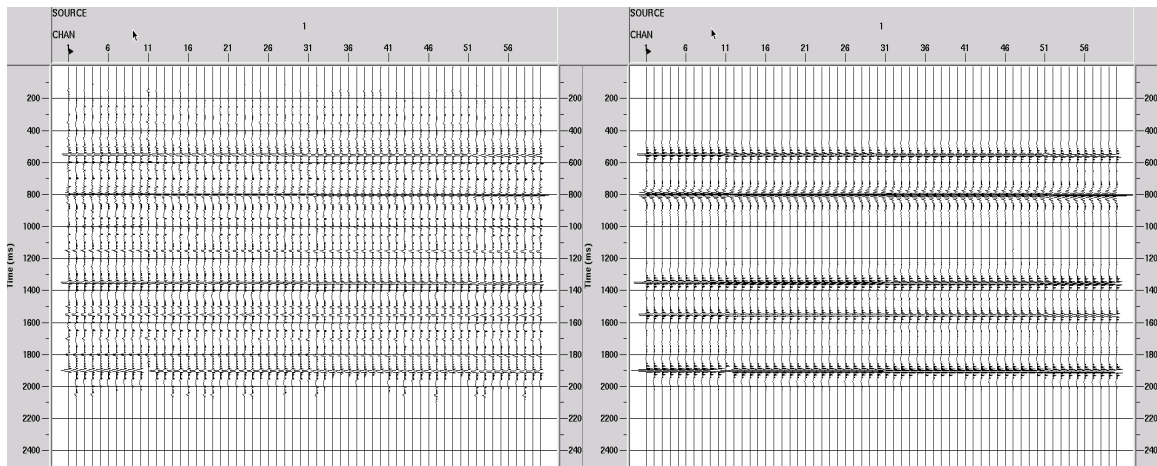
FIG. 12. Model 4—simulated PP gather with five reflection events (left) vs. simulated PS gather with five PS events and embedded random statics (right). Only the PP event at 500 ms and the PS event at approx. 800 ms are the same.



Model 4—cross-correlations and the raw PS gather

FIG. 13. Model 4—raw cross-correlations between matching traces of the PP and PS gathers of Figure 12 (left) vs. the original PS gather. Note the many secondary peaks and side-lobes on these correlations, not all of which are captured by the 1200 ms correlation length.

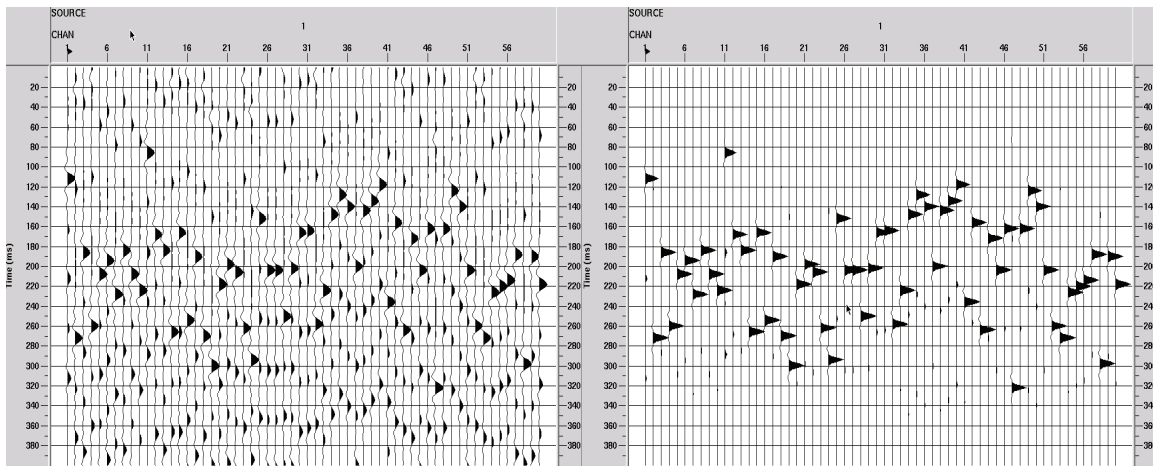
The resulting complexity of the cross-correlations is evident. The corrected PS gather is shown in Figure 14 for both the raw cross-correlations and the conditioned cross-correlations. While the statics are successfully removed by inverse filters derived by both, the introduction of spurious events on the PS gather has become significant, with the possible misidentification of some of these events with legitimate ones, due to their comparable amplitudes. Again, conditioning the correlations greatly improves the resulting statics deconvolution.



Model 4—PS traces corrected using raw correlations (left), and 'conditioned' correlations (right)

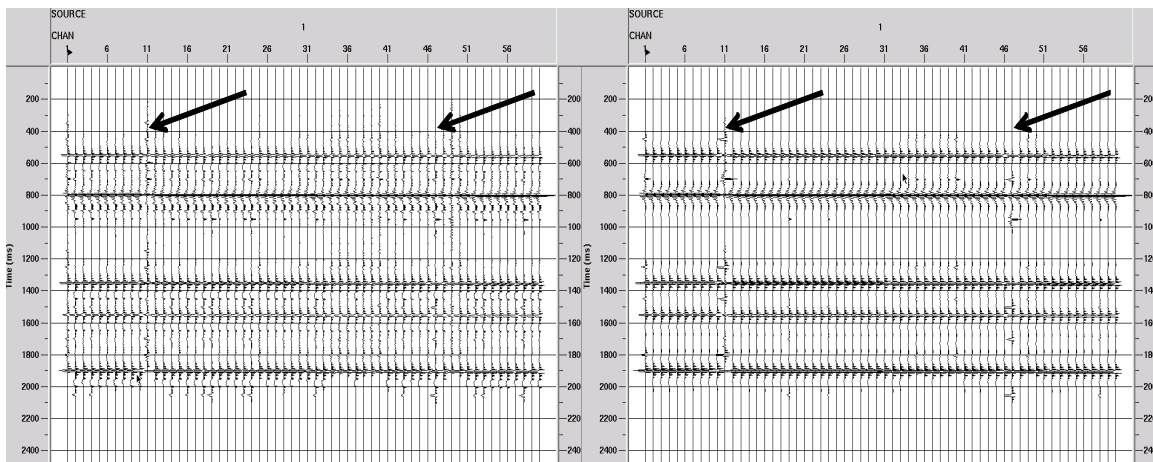
FIG. 14. Model 4—PS gathers corrected by inverse filters derived from the raw correlations in Figure 13 (left), and from the same correlations after 'conditioning' (right). As in Model 3, the conditioning of the correlation functions greatly suppresses spurious events on the deconvolved PS gather.

Another possible approach to reducing the introduction of spurious events into the deconvolved results is to shorten the cross-correlation window, so that fewer secondary peaks are generated (the window must still be greater than or equal to the desired correlation length). Such a set of raw correlations is shown in Figure 15, along with the corresponding conditioned functions. The result of performing the deconvolution with inverse filters derived from each of these two sets of correlation functions is shown in Figure 16. We see that the shorter correlation functions provide cleaner results than the longer ones, with fewer significant spurious events, but that the statics correction itself failed on two of the traces. Applying the conditioning to the shorter correlations cleans up the resulting PS deconvolutions a bit more, but does not repair the statics correction on the two traces.



Model 4—cross-correlations for short window. Raw correlations (left) and ‘conditioned’ correlations (right)

FIG. 15. Model 4—raw cross-correlations for 400 ms window (left) vs. ‘conditioned’ cross-correlations (right) for the same window.



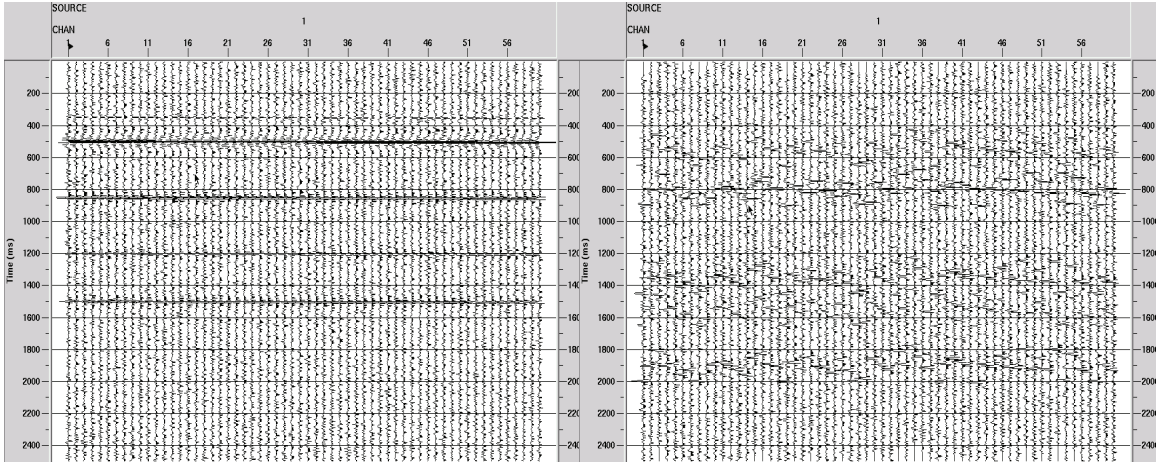
Model 4—PS gather corrected using raw 400 ms correlations (left) and ‘conditioned’ 400 ms correlations (right). Arrows mark bad statics.

FIG. 16. Model 4—PS gather corrected with inverse filters derived from short ‘raw’ cross-correlations (left) vs. short ‘conditioned’ cross-correlations (right). Apparently, shortening the correlation window leads to fewer spurious events in the deconvolved PS gather, but sometimes the statics correction is compromised. Conditioning the cross-correlations suppresses the spurious events even further, but the statics correction still fails on two traces.

Model 5

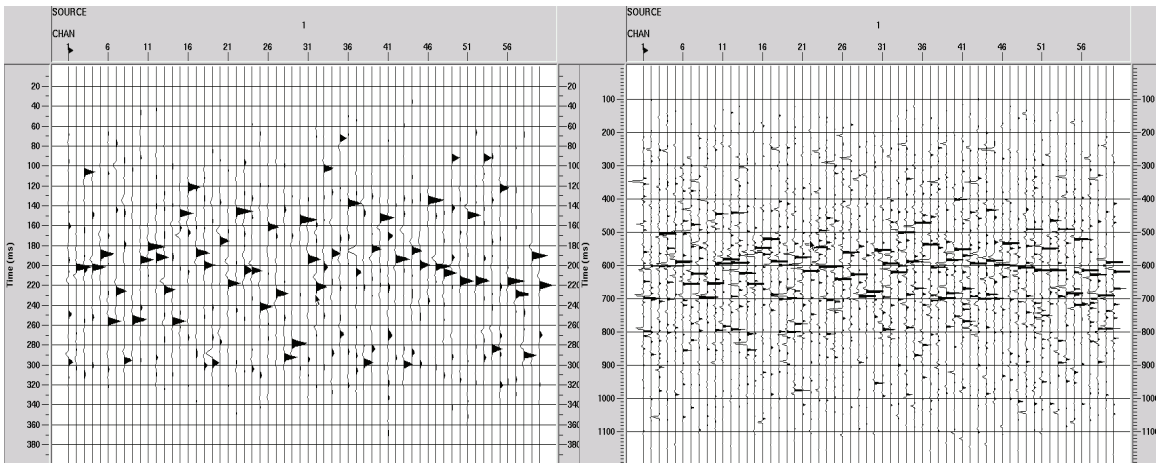
The influence of uncorrelated bandlimited random noise is demonstrated in Model 5. The simulated P and PS events are the same as in Model 4, but significant noise is added to the gathers, as shown in Figure 17. The conditioned cross-correlations are shown in Figure 18 for both 400 ms and 1200 ms correlation lengths; while the deconvolved PS gather for the 400 ms correlation length is shown in Figure 19, with the original unshifted PS gather. The deconvolved PS gather for the 1200 ms correlation length is shown in

Figure 20. These two figures demonstrate that in the presence of random noise, longer correlation length can improve results, but that no coherent spurious events are visible in either case. The longer correlation length appears to ensure that statics are more reliably corrected, both in this noisy model, and in the previous Model 4.



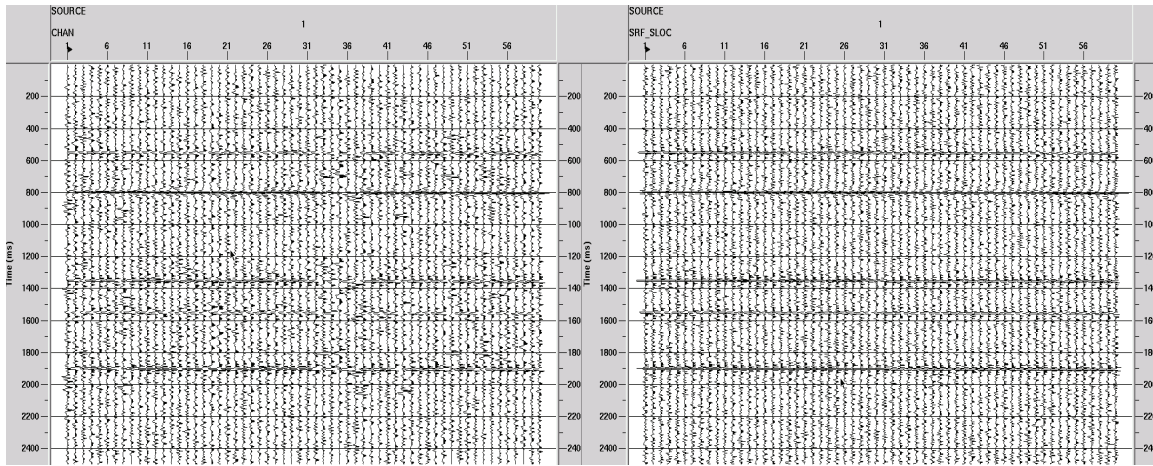
Model 5—same events as Model 4, but random bandlimited noise added. S/N for simulated PP gather is 10.0 (left); S/N for simulated PS gather is 8.0

FIG. 17. Model 5—simulated PP gather with five events and additive bandlimited random noise (left) and its corresponding simulated PS gather, also with five PS events and additive bandlimited random noise (right). As in models 2, 3, and 4, only the PP event at 500 ms and the PS event at approx. 800 ms are matched. Statics are surface-consistent; S/N for the PP gather is 10.0; and S/N for the PS gather is 8.0.



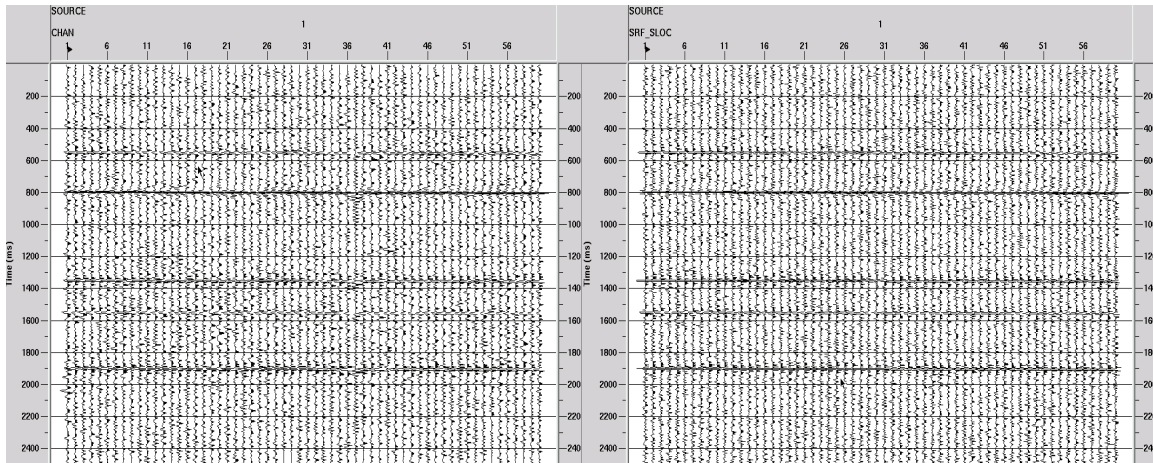
Model 5—conditioned cross-correlations for short 400 ms window (left), and long 1200 ms window (right)

FIG. 18. Model 5—conditioned cross-correlations between the PP and matching PS traces in Figure 17 for a 400 ms window (left) and a 1200 ms window (right).



Model 5—PS gather corrected using 400 ms conditioned correlations (left) vs. original PS gather with no statics (right)

FIG. 19. Model 5—PS gather corrected with inverse filters derived from the 400 ms conditioned cross-correlations (left) vs. the original gather with no statics applied. The statics are mostly good, but phase variations affect parts of some of the events. Spurious coherent events are well-suppressed (at least relative to the noise level).



Model 5—PS gather corrected using 1200 ms conditioned correlations (left) vs. original PS gather with no statics (right)

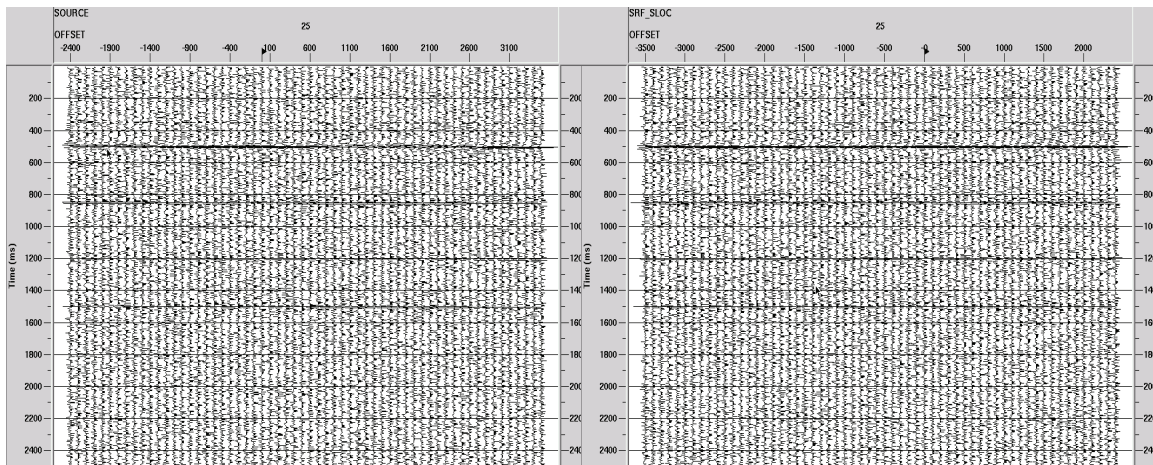
FIG. 20. Model 5—PS gather corrected with inverse filters derived from the 1200 ms conditioned cross-correlations (left) vs. the original gather with no statics applied. The statics are better than with the 400 ms correlations (Figure 19), and spurious events are equally well suppressed (relative to the noise level).

Model 6

This model is the most complex, since it consists of a complete set of shot gathers simulating a seismic survey shot into a fixed receiver spread, for which the shot point moves from one end of the spread to the other. The resulting survey has CDP coverage from one end of the line to the other, with the trace fold reaching a maximum at the centre of the line. Since this is a non-geological model, we compare CDP stacks to evaluate statics-correction success, rather than the more correct CCP stacks, which

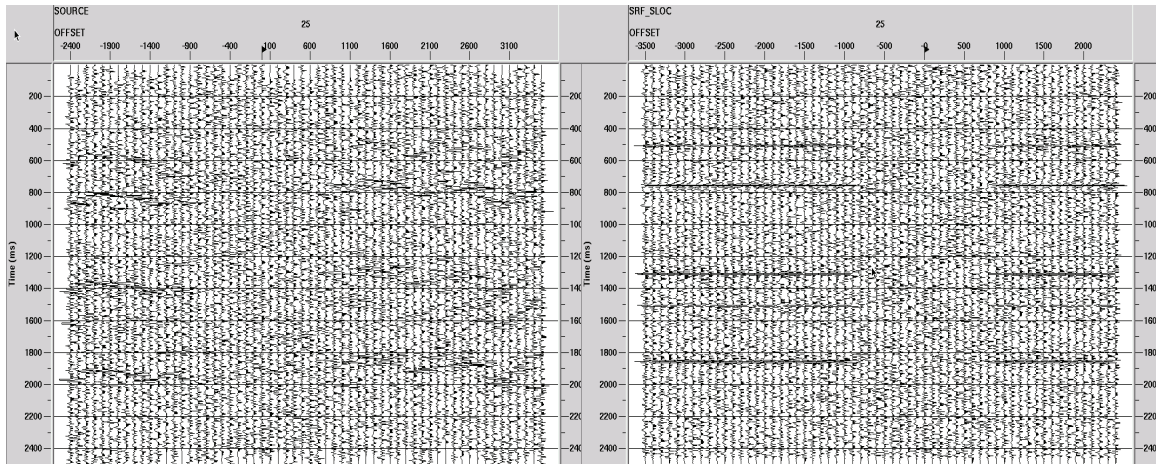
require a velocity model. The reflection events on the PP gathers and the converted wave events on the PS gathers are the same as in the previous two models; but to add realism to the PS gathers, we have zeroed the amplitudes of all simulated converted wave events for offsets between -800 m and +800 m on all gathers. The PS shot gathers were generated in such a way that the receiver statics were the same on each gather (surface-consistent).

We tested both ‘hybrid statics deconvolution’ (cross-correlating PP events with PS events) and the raypath-consistent concept on this model, first by using statics deconvolution on matched pairs of PP and PS shot gathers for the entire line (shot gather interferometry), then by applying the complete raypath interferometry method to the two data sets. Raypath interferometry requires first sorting the data into receiver gathers, so we show in Figure 21 a PP shot gather and a PP receiver gather for the same surface position, and in Figure 22 a PS shot gather and a PS receiver gather, also for the same surface position. Because of the surface-consistency of the PS receiver statics, the PS events are coherent on the receiver gather, but not on the shot gather.



Model 6—PP shot gather (left) and PP receiver gather (right) for surface position 25. S/N for these data is 6.0.

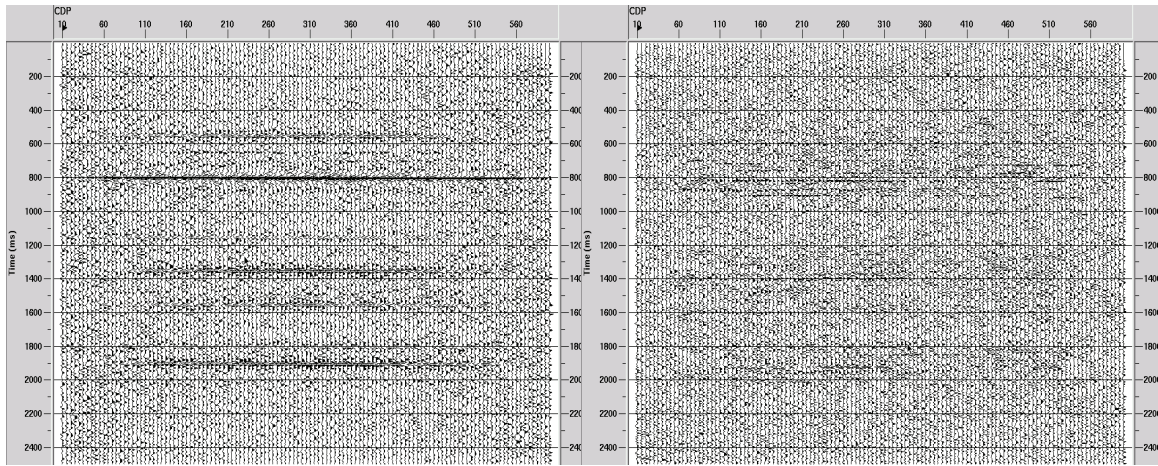
FIG. 21. Model 6—two simulated PP reflected event gathers for surface position 25; shot gather (left), and receiver gather (right). The model has the same five PP events as models 4 and 5, but also contains additive bandlimited random noise with S/N of 6.0.



Model 6—PS shot gather (left) and PS receiver gather (right) for surface location 25. S/N is 6.0 for these data.

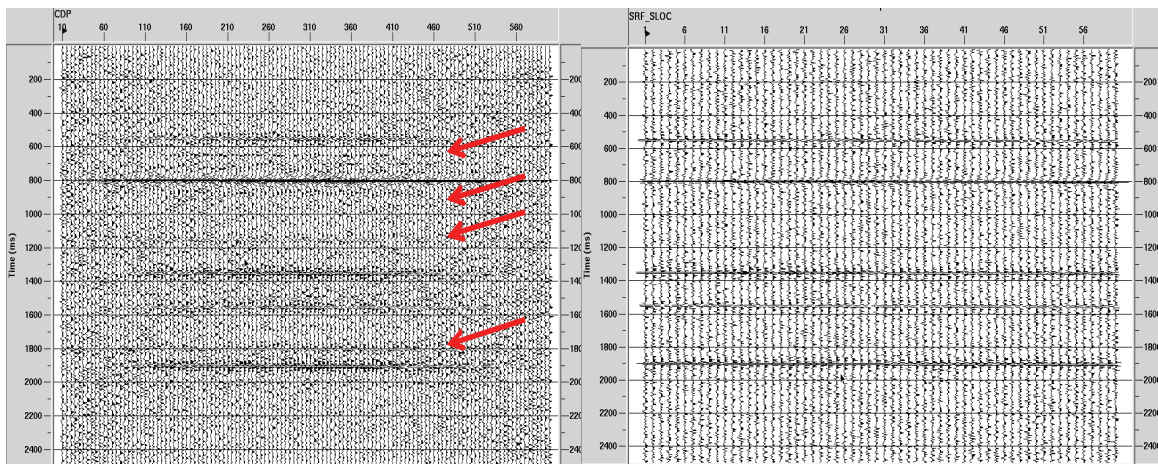
FIG. 22. Model 6—two simulated PS event gathers for surface position 25; shot gather (left), and receiver gather (right). The model has the same five PS events as models 4 and 5, and only the PS event at approx. 800 ms corresponds to a PP reflection event (500 ms). The event amplitudes are zeroed for offsets between -800 m and +800 m to more nearly simulate actual PS events. Since the statics are surface-consistent, the events are coherent on the receiver gather, but not on the shot gather. The S/N of the random bandlimited noise added to these data is 6.0.

The statics deconvolution method applied to pairs of PP and PS shot gathers is just as described above for previous models—we cross-correlated PP and PS traces corresponding to the same receiver position, conditioned the cross-correlation, derived inverse filters, and apply the inverses to the raw PS traces to correct the trace statics. When this procedure is applied to all the paired PP and PS shot gathers in the model and the resulting deconvolved PS shot gathers are stacked by CDP, the results are as shown in Figure 23, compared to the CDP stack of the uncorrected PS gathers. It is evident that we have removed the statics from the simulated PS data well enough that residual statics are not visible on the stacked section. When we compare the same PS stack with a raw, static-free PS gather, however, as in Figure 24, we observe at least four relatively strong and coherent spurious events in addition to the legitimate PS events in the input gathers; and the amplitude of these spurious events is not much smaller than that of some of the legitimate ones.



Model 6—CDP stack of PS shot gathers corrected using shot gather correlations (left) vs CDP stack of uncorrected PS shot gathers

FIG. 23. Model 6—CDP stack of PS shot gathers corrected using the previously-described shot gather statics deconvolution method (left) vs. a CDP stack of the uncorrected gathers.

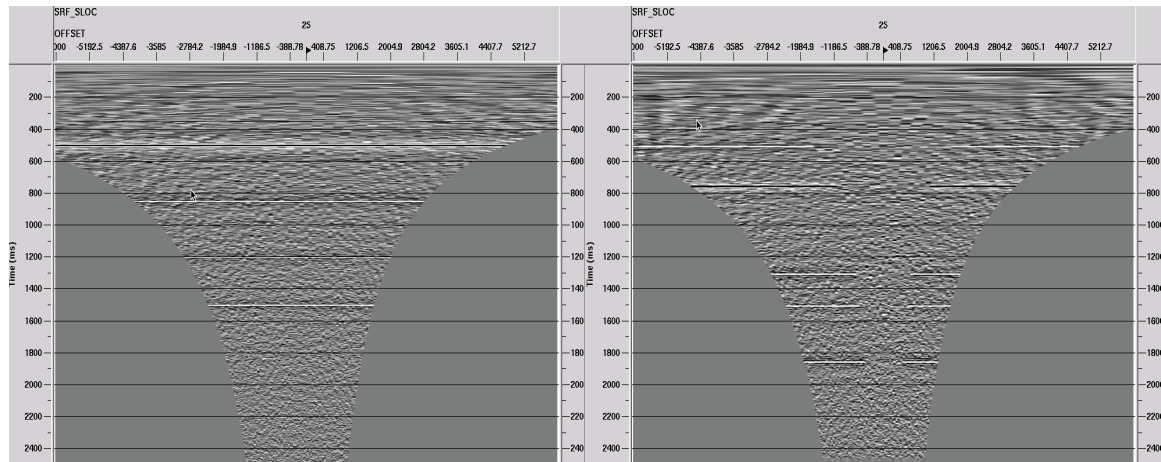


Model 6—CDP stack of PS shot gathers corrected using shot gather correlations (left) vs PS shot gather (no differential statics). Spurious events can be seen on the stack, compared to the receiver gather (red arrows)

FIG. 24. Model 6—comparing the CDP stack of corrected PS gathers (left) with an individual no-statics PS receiver gather (right) in order to identify spurious events on the CDP stack introduced by the statics deconvolution procedure. It is obvious that the statics are being corrected; but we can see some spurious events on the stack, in spite of having used ‘conditioned’ cross-correlations to derive the inverse filters used to deconvolve the individual trace gathers. Evidently, though the spurious events are suppressed on individual gathers, the CDP stack enhances their amplitude enough to make them visible (red arrows).

To pursue the raypath-consistent interferometry technique, we first transformed all the P and PS receiver gathers into the radial trace (RT) domain, as shown in Figure 25. We chose to oversample in the RT domain (large number of traces in the RT transform) in order to build in some redundancy in the separate statics deconvolution solutions applied

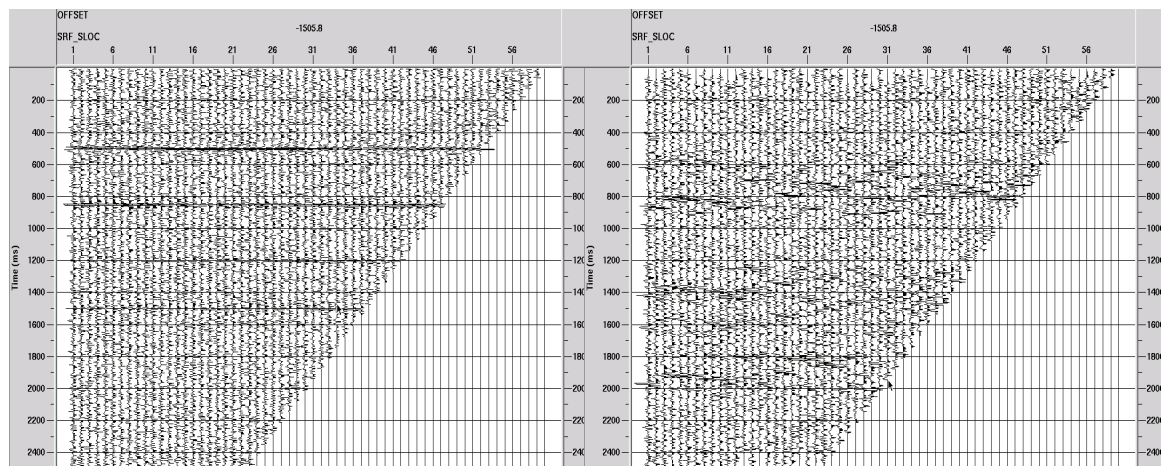
to each common-angle gather. The radial trace transform aperture velocity range is chosen so that every radial trace contains at least one legitimate event. Note that the P and PS events are clearly coherent on the RT trace gathers in this domain.



Model 6—Radial trace transforms of PP receiver gather (left) and PS receiver gather (right)

FIG. 25. Model 6—radial trace transforms of a simulated PP receiver gather (left) and a PS receiver gather (right) for surface location 25.

Next we sorted the RT data into common-angle (or common-raypath) panels, which is done by simply sorting the RT gathers by apparent velocity (raypath angle) and receiver location. Corresponding common-angle gathers for apparent velocity -1505 m/s are shown in Figure 26.

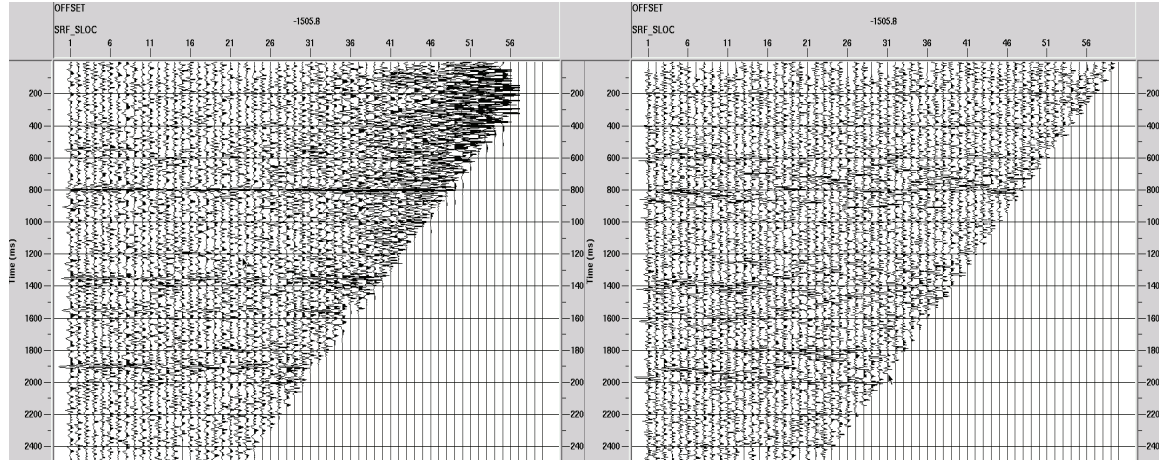


Model 6—common angle gathers for PP data (left) and PS data (right) for the apparent velocity of -1505 m/s

FIG. 26. Model 6—common angle gathers for simulated PP reflected events (left) and simulated PS events (right) for apparent velocity (angle) -1505 m/s.

The procedure for correcting the PS common-angle gathers is exactly the same as for PS shot gathers. Traces from the PP and PS common-angle gathers are matched by receiver

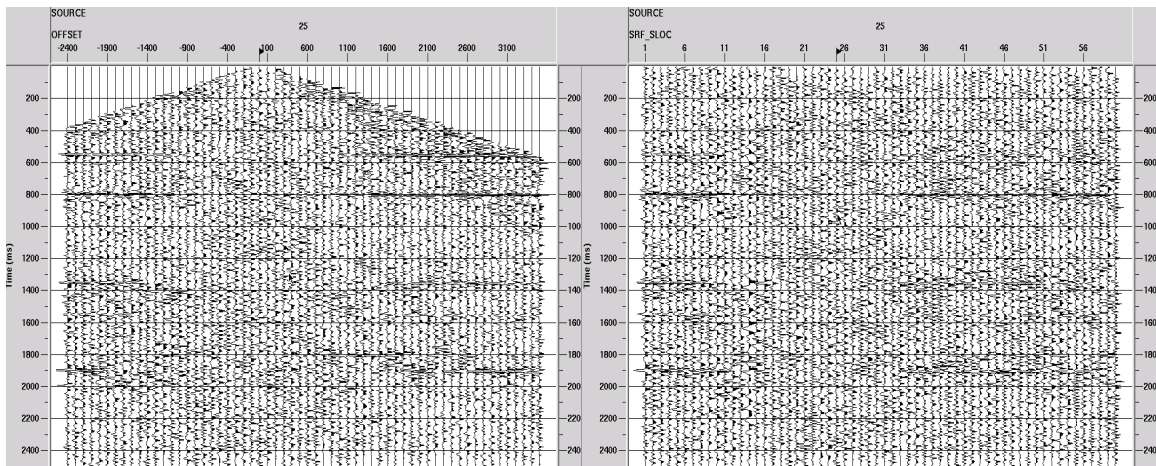
location and cross-correlated. The correlations are conditioned and inverse filters derived for them. The application of the inverse filters to the corresponding traces of the common-angle PS gather corrects the traces. Figure 27 shows the deconvolved PS common-angle gather next to the uncorrected PS common-angle gather. In spite of the noise, the improvement in event alignment is evident.



Model 6—corrected PS common angle gather (left) vs. original common angle gather (right) for the apparent velocity of -1505 m/s

FIG. 27. Model 6—deconvolved PS common angle gather (left) vs. original PS common angle gather (right), for apparent velocity -1505 m/s. While the corrected gather is noisy, it can be seen that the PS events are better aligned (statics corrected).

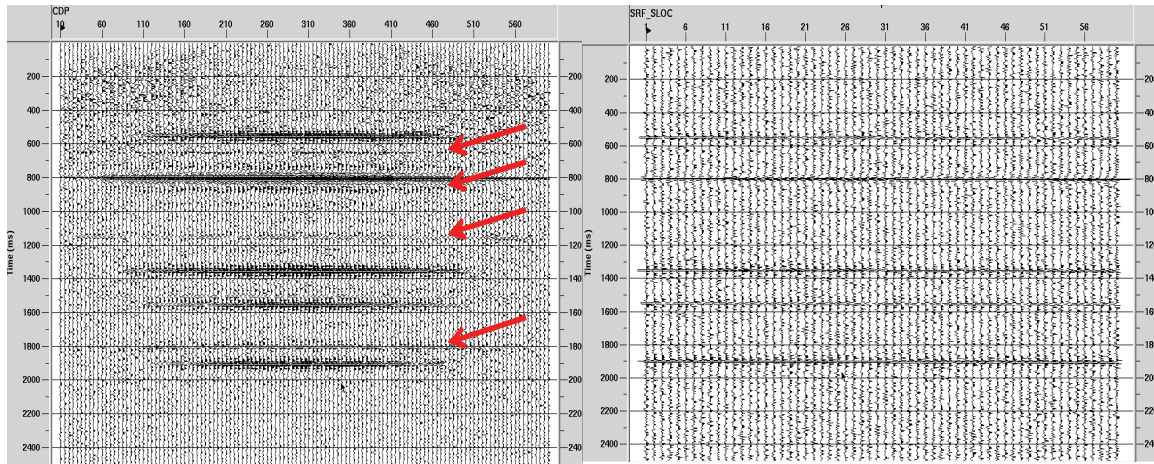
To complete the process, the corrected common-angle gathers are re-sorted into receiver domain radial trace gathers, the RT gathers are inverted to X-T domain receiver gathers, and the data are CDP stacked. As an interesting comparison, Figure 28 compares a PS shot gather corrected using raypath interferometry with the same shot gather using the previously described shot gather interferometry. The former appears to provide a more robust solution, particularly for the shallow events. The apparent ‘muting’ of the early portions of the traces of the raypath-consistent result is an artefact of the choice of radial trace transform aperture, includes none of the model events and thus has no consequence for the results.



Model 6—PS shot gather corrected using raypath interferometry (left) vs the same PS gather corrected using shot gather interferometry (right)

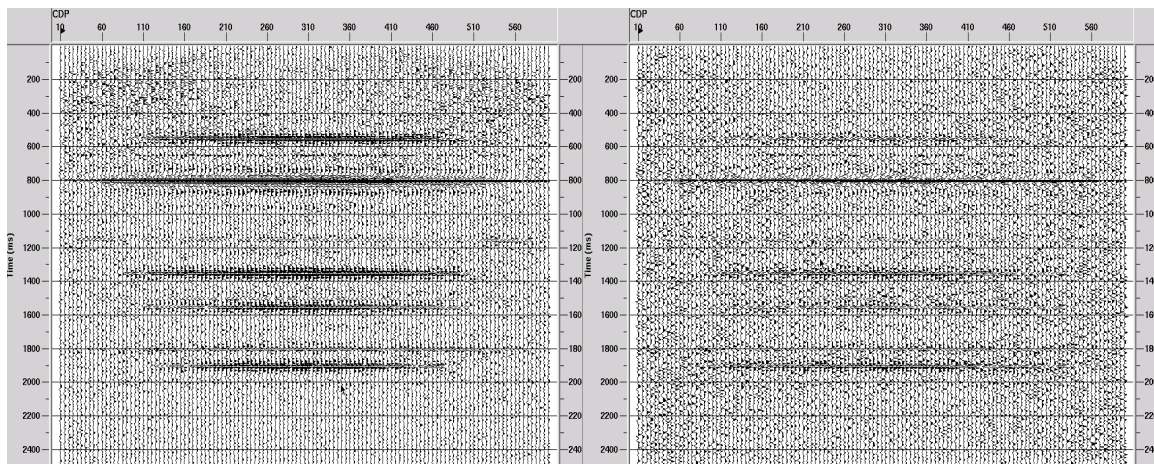
FIG. 28. Model 6—PS event shot gather corrected using raypath interferometry (left) and shot gather interferometry (right). Events are stronger and better aligned with the raypath approach. Early muting on the raypath interferometry result is a consequence of the radial transform aperture, and only random noise has been lost.

Figure 29 compares the CDP stack of the PS gathers corrected using the raypath interferometry method with a raw PS ‘statics-free’ gather (for event identification), and Figure 30 compares the two CDP stacks of the PS data, corrected using raypath interferometry and shot gather interferometry, respectively. The legitimate events have much greater amplitude after raypath interferometry, relative to spurious events, than after shot gather interferometry. On the raypath-consistent stack, we have little difficulty distinguishing legitimate events from spurious ones (based primarily on amplitude). Were we to normalize the event amplitude across the display, we would find that the spurious event amplitudes diminish with increasing stack fold at the centre of the display.



Model 6—CDP stack of PS gathers corrected using raypath interferometry (left) vs single PS shot gather with no statics (right) for event comparison.

FIG. 29. Model 6—CDP stack of PS gathers corrected using raypath interferometry (left) vs. a single PS shot gather with no statics (right). Red arrows mark spurious events.



Model 6—CDP stack of PS gathers corrected using raypath interferometry (left) vs CDP stack of PS gathers corrected using shot gather interferometry (right).

FIG. 30. Model 6—CDP stack of PS gathers corrected using raypath interferometry (left) vs. CDP stack of PS gathers corrected using shot gather interferometry (right). Since the spurious events on both stacks are similar in amplitude relative to each other, and the legitimate events are much stronger on the stack using raypath interferometry, the spurious events are much weaker relative to the legitimate PS events when raypath interferometry is used.

DISCUSSION

From the above results, it appears that, with some limitations, we can, indeed, detect and remove the differences between PP and PS receiver statics for converted wave data at each receiver station by cross-correlating windowed portions of corresponding reflected/converted wave data traces and applying inverse filters derived from the cross-correlations to the raw traces. We can do this either in the original shot domain, or in the

receiver radial trace domain, with the latter showing an advantage for low S/N. The methods we have demonstrated assume that we can correct the PP data (vertical component) for statics prior to using them in these procedures, and that both PP and PS (inline component) are corrected for NMO. Furthermore, we relegate geological structure preservation (the corrected PS data will assume structure intrinsic to the PP data) to future work, as well as details of intrinsic reflectivity or ‘convertivity’ and their role in interferometry.

In all the models above, when we matched a PP reflected event with its corresponding PS converted wave event, the resulting cross-correlations were dominated by the relative shift between the matched events, enabling us to derive appropriate inverse filters for removing the detected relative trace shifts. With the more complicated models, as we expected, secondary correlation peaks appeared and led to spurious events in the deconvolved converted wave output. Processing tactics can be adopted that diminish the effects of these spurious events: ‘conditioning’ the cross-correlation functions by raising samples to an odd exponent, followed by Hanning weighting the functions, whitens the cross-correlations without adding new peaks. This leads to inverse filters which are much more localized and give rise to fewer and weaker spurious events when deconvolving the PS traces. Shortening the correlation window to allow only those correlation peaks within the probable range of PS wave receiver statics is another trick which diminishes the amplitude of spurious events on the deconvolved traces.

The introduction of bandlimited random noise adds some complications. The presence of the noise can lead to cross-correlation functions whose inverse filters do not always correct the embedded statics in the converted wave data, even when the correlations are ‘conditioned’. In this case, longer correlation windows, rather than shorter, can lead to more robust solutions without significantly amplifying spurious events. This is a trade-off, however, and at some point, the spurious events become too significant to ignore.

When we look at our most sophisticated model--the complete 2D line--we discover that if we use the simplest approach, correlating traces on corresponding shot gathers, the statics are corrected, but the CDP stack image contains spurious events with significant amplitude, due to being enhanced by the stacking process. Thus, the raypath-consistent method is favoured because of its inherent redundancy.

ACKNOWLEDGEMENTS

The author acknowledges the ongoing support of CREWES sponsors and staff.

REFERENCES

- Bakulin, A. and Calvert, R., 2006, The virtual source method: theory and case study, *Geophysics*, **71**, S1139-S1150.
- DeMeersman, K., and Roizman, R., 2009, Converted wave receiver statics from first break mode conversions: 2009 CSPG CSEG CWLS Convention, expanded abstracts.
- Henley, D.C., 2004, A statistical approach to residual statics removal: CREWES 2004 research report, **16**.
- Henley, D.C., 2005, Raypath-dependent statics: CREWES 2005 research report, **17**.

- Henley, D.C., 2006, Application of raypath-dependent statics to Arctic seismic data: CREWES 2006 research report, **18**.
- Henley, D.C., and Daley, P.F., 2007, Connecting statics deconvolution and seismic interferometry: CREWES 2007 research report, **19**.
- Henley, D.C., 2007, Raypath statics revisited: new images: CREWES 2007 Research Report, **19**.
- Henley, D.C., 2008, Raypath interferometry: statics in difficult places: 2008 CSPG CSEG CWLS Convention, expanded abstracts.
- Henley, D.C., and Daley, P.F., 2008, Applying interferometry to converted wave statics: CREWES research report, **20**.
- Henley, D.C., and Daley, P.F., 2009, Hybrid interferometry: surface corrections for converted waves: CREWES research report, **21**.
- Wapenaar, K., Draganov, D., and Robertsson, J., 2006, Introduction to the supplement on seismic interferometry: *Geophysics* **71**, No. 4, S11-S14.